Applied Biological Research 27(2): 223-233; (2025)
DOI: 10.48165/abr.2025.27.01.22

MOLECULAR TRANSPORT BY VARYING THE SIZE OF NANOPORE IN THE MEMBRANE OF GUV USING SIMULATION

Thuhedur Rahman[1], Md. Asaduzzaman[1], Shahariar Emon[1], Md. Imran Hossain[1], Md. Saif Ishtiaque[1], Mohammad Abu Sayem Karal[2], Md. Masum Billah[3], Hiromitsu Takaba[4], and Md. Khorshed Alam*[1]

[1]*Department of Physics, University of Barishal, Kornokathi, Barishal - 8254 (Bangladesh)*
[2]*Department of Physics, Bangladesh University of Engineering and Technology, Dhaka - 1000 (Bangladesh)*
[3]*Department of Physics, Jashore University of Science and Technology, Jashore - 7408 (Bangladesh)*
[4]*Department of Environmental Chemistry and Chemical Engineering, School of Advanced Engineering, Kogakuin University, 2665-1 Nakano Hachioji, Tokyo 192-0015 (Japan)*
*****e-mail: *khorshed_du@yahoo.com*

(Received 12 January, 2025; accepted 7 June, 2025)

ABSTRACT

Transient pore formation in lipid membranes plays a critical role in diverse biological and synthetic processes. Understanding the molecular transport mechanism through these membrane pores is a key step in the optimization of drug release, and membrane integrity regulation. In this study we studied the molecular transport through nanopores formed in the membrane of Giant Unilamellar Vesicles (GUVs) using finite element simulation in COMSOL Multiphysics. We explored the impact of nanopore diameter (16-60 nm), fluorescent probe size (R_{SE} 0.74-5.00 nm), on molecular transport. Using Fick's law of diffusion and the Stokes-Einstein equation, we calculated leakage rate constants k_{leak} for various fluorescent probe sizes. Simulations revealed that larger nanopores significantly increased leakage rates, whereas increasing probe size led to slower leakage. Additionally, larger suspension areas accelerated molecular clearance from the vesicle, amplifying overall flux. The model was validated against experimental data on magainin 2-induced pores, showing strong agreement and confirming the accuracy of our approach. These findings provide insight into nanopore-mediated transport and offer a predictive framework for designing membrane-permeabilizing systems in synthetic biology and drug delivery applications.

Keywords: Cell permeabilization, COMSOL, fluorescent probes, giant unilamellar vesicles (GUVs), molecular transport

INTRODUCTION

Cell membranes act as selective barriers that tightly regulate the transport of molecules, maintaining homeostasis and enabling essential biological functions (Sikorska *et al.,* 2012). In both natural and engineered systems, these membranes are often intentionally permeabilized to enable the transport of molecules across them (Casas-Rodrigo *et al.,* 2025). Such permeabilization lies at the core of diverse biomedical techniques, from intracellular drug and gene delivery to biosensing and membrane biophysics (Nayak and Herzog, 2010;, Vargason *et al.,* 2021; Liu *et al.,* 2024). However, in a permeabilized cell, the molecular transport is inherently bidirectional. Whenever pores are formed, whether by physical means like electroporation, chemical agents, or biologically active peptides, they allow not only the influx of molecules but also the leakage of internal contents (Tamba and Yamazaki, 2005; Karal Alam *et al.,* 2015; Casciola and Tarek, 2016; Stewart *et al.,* 2016). In

cellular systems, this leakage can include cytosolic enzymes, ions, or fluorescent tracers, and it must be carefully controlled to ensure cell viability and delivery specificity. In drug delivery applications using liposomes or unilamellar vesicles, release through transient pores is the actual mechanism by which therapeutics are delivered at the target site. Thus, understanding the dynamics of leakage through transient nanopores is essential. not only to avoid unintended cytotoxicity in cell-based delivery systems but also to optimize the timing and dosage of drug release from synthetic vesicles.

The kinetics of this leakage process are determined by several factors, *viz*., pore size and geometry, membrane properties, molecule size, and external environment. To study the mechanism, researchers have been using model systems such as Giant Unilamellar Vesicles (GUVs), which provide a valuable experimental platform for studying nanopore-mediated transport, offering a controlled environment to investigate molecular interactions under varying physical and chemical conditions (Saitoh *et al.,* 1998; Tanaka *et al.,* 2002; Yamashita *et al.,* 2002). They have been widely used to study formation of pores caused by a variety of membrane-active substances, including antimicrobial peptides (AMPs) (Tamba and Yamazaki, 2009; Tamba *et al.,* 2010; Karal *et al.,* 2015; Hasan *et al.,* 2018), nanoparticles (Roiter *et al.,* 2008), mechanical tension (Karal and Yamazaki, 2015; Karal *et al.,* 2016), electroporation (Sengel and Wallace, 2016; Karal *et al.*,2019; Sözer *et al.,* 2020), cell-penetrating peptides (Zasloff, 2002; Sharmin *et al.,* 2016), and osmotic pressure (Alam Shibly *et al.,* 2016; Ahamed *et al.,* 2022). Additionally, the use of optical microscopy enables the visualization of GUV structure and the observation of fluorescent probe leakage in both temporal and spatial dimensions (Karal *et al.,* 2019), providing advantages over smaller vesicles.

Despite the advantages of GUVs in mimicking the cellular membranes and allowing direct visualization of leakage events, experimental approaches alone face several limitations. A major reason for this is the difficulty in directly observing the nanoscale pores in lipid bilayers (Teissie, 2017; Kotnik *et al.,* 2019). These structures are highly transient and fragile for sample preparation methods required for electron microscopy, such as vacuumization, cryofixation, or metallic coating, which often distort or destroy the pores (Chang and Reese, 1990). Early visual evidence of membrane pores was later debunked as artifacts caused by the preparation methods (Spugnini *et al.,* 2007). Additionally, techniques like total internal reflection fluorescence microscopies have been employed to study ionic flux through individual pores (Sengel and Wallace, 2016). Nevertheless, these methods do not have the necessary resolution to capture the fast dynamics and structural details of pore formation. These limitations make it challenging to measure the precise kinetics of efflux through nanoscale pores. Moreover, direct quantification of key parameters, like pore size, molecule-pore interaction, and the impact of surrounding geometry, is often inaccessible experimentally.

To overcome these limitations, researchers have increasingly employed computational modelling techniques to gain mechanistic insight into membrane transport processes (Boukany *et al.,* 2011; Hasan *et al.,* 2018; Sözer *et al.,* 2020; Rahman *et al.,* 2025; Emon *et al.* 2025). Among these, finite element simulations using software like COMSOL Multiphysics have emerged as a powerful tool for studying diffusion dynamics across complex geometries (Karal *et al.,* 2020; Asaduzzaman *et al.,* 2025). Unlike molecular dynamics simulations, which are limited by high computational costs and small spatial scales, finite element methods allow for the efficient modelling of macroscale transport phenomena such as solute leakage from vesicles over physiologically relevant time scales. Previous computational studies have primarily focused on solute entry into GUVs through fixed-size pores or simplified geometries, often under specific experimental conditions. However, the efflux of molecules from vesicles, especially as a function of nanopore size, probe properties, and external suspension geometry, remain less explored. Yet, this efflux represents a critical aspect of drug release, cytosolic loss in permeabilized cells, and membrane permeability in general. In this study, we addressed this gap by employing a two-dimensional finite element model in COMSOL to simulate molecular leakage from GUVs through a single nanopore. By systematically varying nanopore radius, fluorescent probe size, and external suspension area, we calculated the leakage rate constants (k_{leak}) and evaluated how these parameters shape efflux dynamics. The results were validated against experimental data from magainin 2-induced pores, demonstrating strong agreement.

MATERIALS AND METHODS

Nanopores in the GUV's membrane were modelled using AutoCAD for precise geometry, later analysed in COMSOL Multiphysics. COMSOL simulations, based on the finite element method, accounted for diffusion-driven molecular transport through nanopores, incorporating parameters like probe size and membrane thickness.(Datta and Rakesh 2010). This software employs a system of differential equations to analyse molecular transport, accounting for diffusion, migration, and convection flux through the nanopore (Movahed and Li, 2012).

The simulation assumed that a spherical GUV, represented as a circular 2D membrane with a thickness of 4 nm and a radius of 4 µm (Fig. 1). Molecular suspension area was set to 113 µm² to reflect experimental conditions as depicted in Fig. 1(d). Diffusion through nanopores was modelled using the transport of diluted species feature, with the nanopore geometry tailored for varying probe and pore sizes (Berthier and Silberzan, 2010).

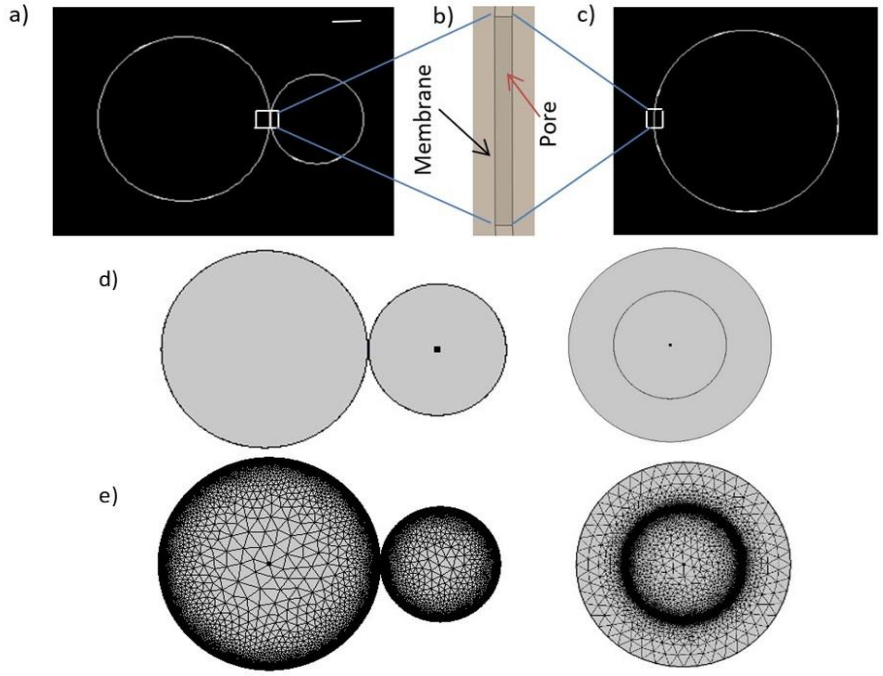

Fig. 1: Nanopore structure in GUV membrane, (b) Zoomed-in views of a solitary nanopore within the GUV membrane (a, c) was crafted utilizing AutoCAD. (d) The membrane geometry was modelled in 2D for COMSOL simulation; (e) Visual representation of a standard mesh for a single GUV modelled in COMSOL. Scale bar: 5 nm (b), and 5 µm (a, c).

Simulations were designed to match the experimental parameters, ensuring comparability. Nanopore radii, ranging from 16 to 60 nm (Fig. 1b), were selected based on experimental data for GUVs with a 4 µm dia. Time-dependent changes in molecular concentration were tracked to derive transport kinetics, using fluorescence intensity as a proxy for molecular entry. The simulation incorporated a membrane thickness of 4.0 nm, which aligns with previous reported values (Rawicz *et al.*, 2000).

The analysis of the transportation of molecules through the nanopore and into the GUVs was conducted by the principle of diffusion driven by Fick's law (Gaur *et al.* 2014) as follows:

$$R_i = \frac{dC_i}{dt} + \nabla.(-D_i.\nabla C_i), \qquad (1)$$

where, R_i represents the rate of reaction for the i^{th} species, C_i represents the molecular concentration of the i^{th} species in the solution, and D_i denotes the diffusion coefficient of fluorescent probes within

the solution of i^{th} species. An analogous equation has been used previously in COMSOL Multiphysics to study the molecular transportation through a singular nanopore formed via electroporation (Gómez *et al.*, 2014; Jayasooriya and Nawarathna, 2017) and nanopores created by magainin-2 (Karal *et al.*, 2020). The correlation between D_i, the coefficient of diffusion and R_{SE} (nm), the radius as per Stokes-Einstein equation for fluorescent probes in aqueous solution at 25°C is as follows (Tamba *et al.* 2010):

$$D_i = \frac{k_B T}{6\pi\eta R_{SE}} = \frac{2.45 \times 10^{-19}}{R_{SE}} (\mathrm{m}^2/\mathrm{s}), \qquad (2)$$

In equation, there are additional symbols and their corresponding values: k_B represents Boltzmann constant ($k_B = 1.38\times10^{-23}$ J/K), T represents the temperature in Kelvin (T = 298 K), and η represents the viscosity of water ($\eta = 8.90\times10^{-4}$ Pa·s).

The diffusion coefficients (D_i) and Stokes-Einstein radii (R_{SE}) of fluorescent probes used in this study were:

Fluorescent probes	R_{SE} (nm)	$D_i \times 10^{-10}$ (m^2/s)
Calcein	0.74	3.31
TRD-3k	1.4	1.75
TRD-10k	2.7	0.91
AF-SBTI	2.8	0.88
FITC-BSA	3.6	0.68
TRD-40k	5.0	0.49

The simulation incorporated key components: GUV interior, lipid membrane, and aqueous nanopore. Assumptions included uniform permittivity of 80 within the pore, reflecting bulk water properties at25°C. This ensured consistency with experimental conditions and facilitated accurate modelling of molecular flux (Karal*et al.*, 2015). However, in our recent publication, a slightly elevated relative permittivity value for body fluid was employed (Roy *et al.*, 2019). To study molecular transport with COMSOL, it was essential to define the concentration of source in cytoplasm, which was set at 1.0 mol m^{-3} to represent the concentration of probes. A narrow diffusion barrier with a thickness of 1.0 nm and a diffusion coefficient of 0 m^2 sec^{-1} was incorporated at the interior layer of GUV membrane, along with other selected boundaries. The outer concentration surrounding the GUV was set to 0 mol m^{-3}. A standard mesh configuration, as illustrated in Fig. 1e, was employed for the simulation. Simulations tracked temporal variations in probe concentration within the GUV, providing a basis for deriving leakage rate constants (k_{leak}) and validating transport kinetics against experimental data.

RESULTS AND DISCUSSION

Multiple fluorescent probes transport through a GUV's nanopore

We initiated our study by examining the transport of diverse fluorescent probes into a Giant Unilamellar Vesicle (GUV) via a solitary nanopore. Fig. 2a,b shows the transport of TRD-3k through a 26 nm radius nanopore into a GUV with a 4 μm diameter. Prior to the initiation of molecular transport, a deliberate contrast was maintained between the interior and exterior regions of the GUV, as depicted in Fig. 2a,b at the initial time point (0 sec). This observation aligns with previous findings on molecular transport through nanopores under the influence of an electric field, as studied through COMSOL simulation (Gómez *et al.* 2014, Jayasooriya and Nawarathna 2017). The fluorescence intensity within the GUV is represented using a color gradient spanning from 0 (blue) indicating the lowest intensity to 1.0 (red) indicating the highest fluorescence intensity.

The time-dependent changes in normalized fluorescence intensity within GUV for TRD-3k (Fig. 2a,b), provides insights into the molecular transport rate. Fig. 2c specifically showcases the fluorescence intensity observed for TRD-3k, demonstrating a gradual decrease over time until it reaches a steady value at 13 sec. Similar experiments were conducted using other fluorescent probes

like calcein, TRD-10k, AF-SBTI, FITC-BSA, and TRD-40k. Notably, all these probes demonstrated a consistent trend of decreasing fluorescence intensity over time. Fluorescence intensity saturation occurs when normalized intensity drops to zero. Fig. 3a confirmed that molecular entry rate decreases with larger probe sizes.

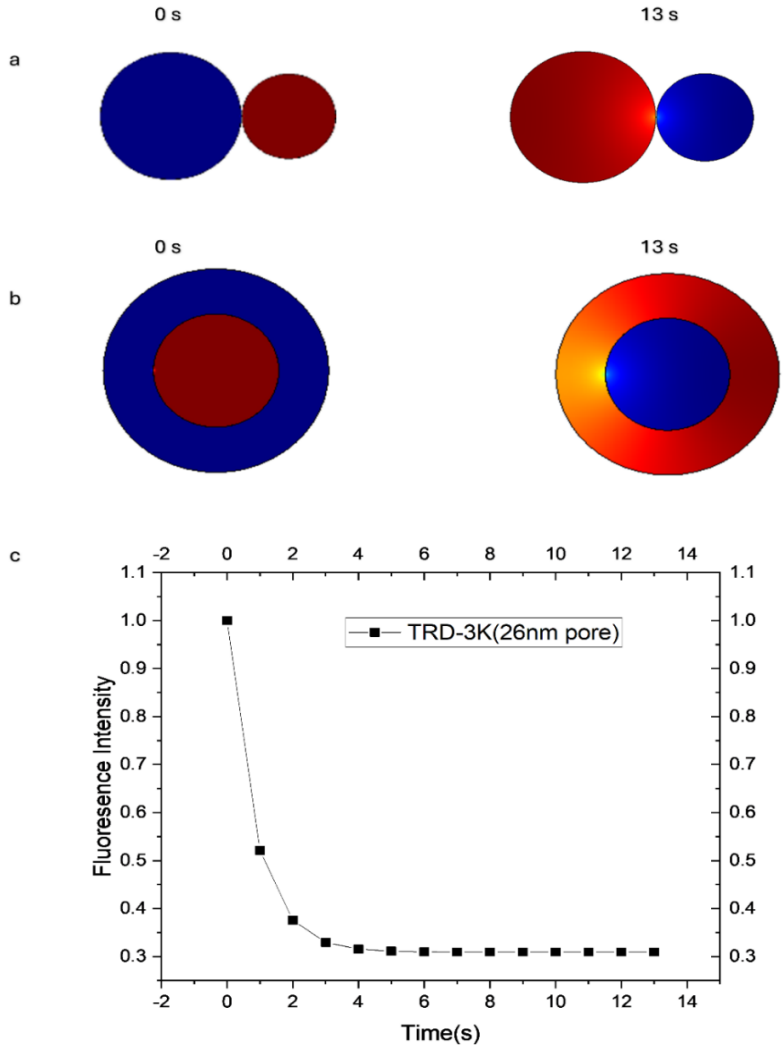

Fig. 2: a) and b) illustrate the transport of TRD-3k through a 26 nm nanopore into 4 µm GUV. The fluorescence intensity changes reveal the molecular transport rate, with higher intensities indicating greater transport. c) shows the change in normalized fluorescence intensity within GUV with time for TRD-3k. An exponential growth function (solid line) of Eq. (4) is fitted to time dependent fluorescence intensity.

The rate constant k_{leak} for fluorescent probe leakage was determined by using Eq. 3 and normalized fluorescence intensities by Eq. 4 fitted to the data in Fig. 2c (Tamba *et al.* 2010):

$$C^{in}(t) = C_0^{in} exp(-k_{leak} t), \quad (3)$$

$$FI^{in}(t) = FI_0^{in} exp(-k_{leak}\, t), \quad (4)$$

The process follows single-exponential decay kinetics, where saturation time and k_{leak} are directly related. In this study, we focused on the representative rate constant for molecular transport through the single pore. The obtained leakage rate constant (k_{leak}) values for various fluorescent probes are presented in Table 1. The Fig. 3a,b illustrates that k_{leak} decreased with probe size and increased with suspension area. These trends highlight the critical role of nanopore size, probe size, and suspension area in determining the transport kinetics. Larger nanopores facilitated faster transport, while increased suspension areas enhanced molecular flux, underscoring the potential for optimizing experimental configurations for specific applications. The relationship between nanopore size and transport kinetics was consistent with predictions from diffusion coefficients, as larger pores reduced resistance to molecular movement (Karal *et al.*, 2020; Asaduzzaman *et al.*, 2025).

Table 1: The k_{leak} values derived for different fluorescent probes for size of the GUV's pore

Probe / Diameter (nm)	Calcein		TRD-3K		TRD-10K		AF-SBTI		FITC-BSA		TRD-40K	
	2 GUV	Circle	2 GUV	Circle	2 GUV	Circle	2 GUV	Circle	2 GUV	Circle	2 GUV	Circle
16	0.19	0.19	0.089	0.089	0.029	0.029	0.036	0.036	0.026	0.026	0.024	0.024
18	0.26	0.26	0.12	0.12	0.042	0.042	0.048	0.048	0.036	0.036	0.028	0.028
20	0.32	0.32	0.14	0.14	0.055	0.056	0.06	0.06	0.048	0.049	0.031	0.031
24	0.34	0.35	0.165	0.165	0.069	0.069	0.75	0.75	0.072	0.072	0.046	0.046
25	0.36	0.36	0.175	0.175	0.082	0.083	0.097	0.097	0.079	0.079	0.050	0.050
26	0.38	0.38	0.19	0.19	0.095	0.095	0.12	0.12	0.086	0.086	0.055	0.055
32	0.51	0.51	0.25	0.25	0.12	0.12	0.15	0.15	0.11	0.11	0.06	0.06
38	0.61	0.61	0.31	0.31	0.15	0.15	0.17	0.17	0.13	0.13	0.10	0.11
39	0.63	0.63	0.315	0.315	0.155	0.155	0.19	0.20	0.135	0.135	0.105	0.105
40	0.65	0.65	0.32	0.32	0.19	0.20	0.20	0.21	0.14	0.14	0.11	0.11
44	0.67	0.67	0.34	0.34	0.175	0.176	0.215	0.215	0.15	0.16	0.12	0.12
46	0.69	0.69	0.38	0.39	0.185	0.185	0.25	0.25	0.165	0.165	0.13	0.13
60	0.74	0.75	0.45	0.45	0.21	0.21	0.32	0.32	0.20	0.20	0.14	0.14

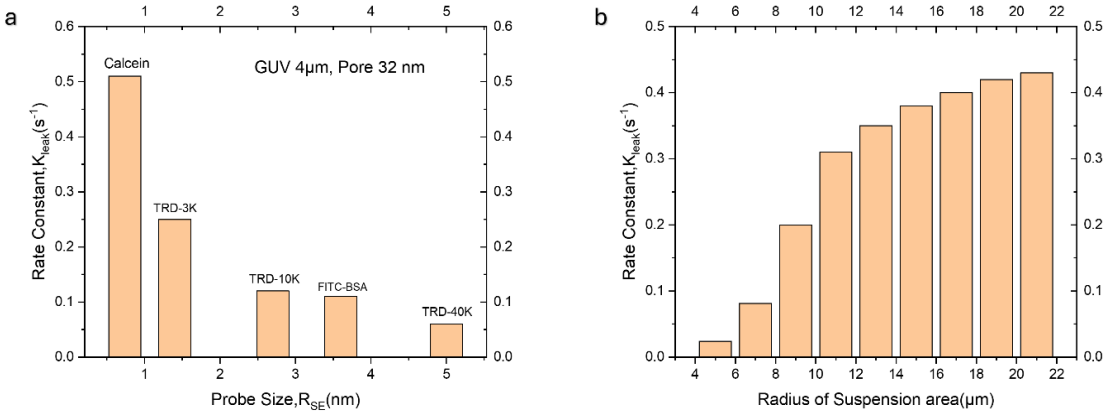

Fig. 3: The bar diagrams in (a) and (b) respectively are the fluorescent probe (R_{se}) dependent rate constant and suspension area dependent rate constant of molecular transport through 32 nm pore with GUV size 4 μm

Analysing simulation findings against experimental data

The study compared experimental transport data of fluorescent probes in DOPG/DOPC (5/5)-GUVs to COMSOL simulations, focusing on magainin 2-induced pores (Tamba *et al.* 2010). Fig. 4 highlights strong agreement between simulated and experimental results, validating the predictive accuracy of the model and its applicability for analysing molecular transport dynamics.

Comparison of simulation outcomes with alternative computational models

We investigated the transport of fluorescent probes into Giant Unilamellar Vesicles (GUVs) using a single nanopore, varying the nanopore sizes from 16 to 60 nm. Similarly, another study focused on molecular transport of fluorescent probes through a nanopore, specifically examining a fixed size (Karal *et al.* 2020). Further understanding of molecular transport through a nanopore under the influence of an electric field was achieved using COMSOL simulations (Jayasooriya and Nawarathna 2017). Similar results were observed consistently for each case with a fixed size of nanopore and GUV.

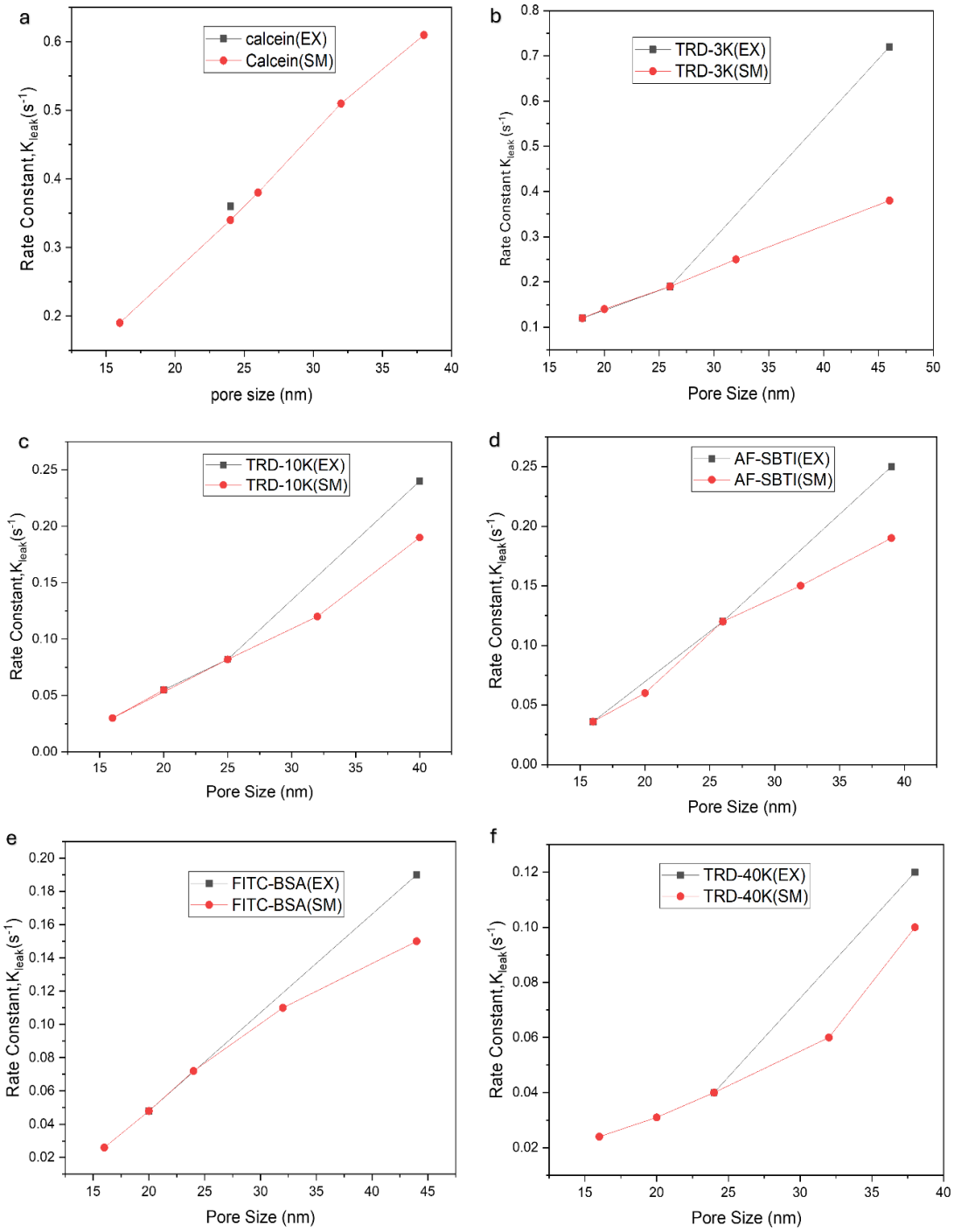

Fig. 4: Comparison of simulation and experimental data for various fluorescence probes

In present work, we used circular suspension area but in previous work the suspension area was considered as square (Karal *et al.* 2020).

Analytical analysis of transport of molecules through the GUV's nanopore

A theoretical equation was used to relate the rate constant of fluorescent probe leakage with the cross-sectional area of magainin 2-induced pores. This model assumed that the fluorescent probes exclusively penetrate through the magainin 2-induced pores, moving from inside to outside of the

GUV. The membrane permeability, representing the substance flux per unit area of the pores (J. mol $m^{-2}\cdot sec^{-1}$), is governed by Fick's law:

$$J = -P\left[C^{in}(t) - C^{out}(t)\right] = -\frac{D_i}{h}\left[C^{in}(t) - C^{out}(t)\right] \quad (5)$$

The permeability coefficient (P) for the substance within the pore is calculated as the ratio of the diffusion coefficient (D) of the substance in pores relative to the effective pore length, approximately equivalent to the membrane width (h = 4 nm). The rate of fluorescent probe leakage from a GUV, under the assumption of a concentration outside the GUV (C^{out}) = 0 throughout, can be articulated as follows (Tamba and Yamazaki 2009):

$$\frac{C^{in}(t)}{C_0^{in}} = exp(-k_{leak}t) \quad (6)$$

Where, k_{leak} = K D_i S_p/Vh. Given that, h = 4 nm, $S_p = \pi r^2$ (r is pore's radius), $V = \pi d^3/6$ (d is GUV's diameter) and $D_i = 2.45\times10^{-19}/R_{SE}$ (m^2 sec^{-1}); thus, we can write it as:

$$k_{leak} = K\,\frac{3.7\times10^{-10}r^2}{R_{SE}d^3}(s^{-1}) \quad (7)$$

In our 2D simulation system, equation 7 can be adjusted as follows:

$$k_{leak} = K\frac{0.77\times10^{-10}\,l}{R_{SE}d^2}(s^{-1}) \quad (8)$$

Eq. 8 demonstrates that k_{leak} depends on pore size (2r), probes (R_{SE}) and diameter of the GUV (d). By maintaining a constant GUV diameter, this study isolates the impact of nanopore and probe sizes on transport dynamics, offering a clearer understanding of these critical variables.

To assess the suggested analytical method, it is essential to fit it to the simulation outcomes. In present study, a fitting procedure using the parameter K to match the simulated k_{leak} values for different fluorescent probes and GUVs of different sizes was employed. Fig. 5 confirms the reliability of Eq. 8 in predicting k_{leak} for various probes. The strong correlation between experimental and fitted data

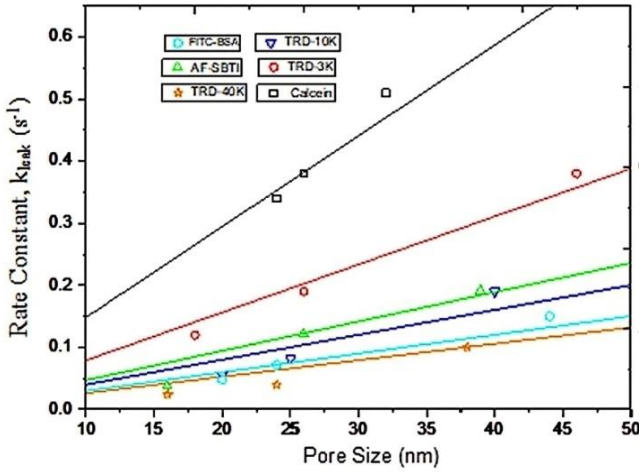

Fig. 5: The rate constant of molecular transport in the GUVs, dependent on pore size, for various fluorescent probes

underscores the model's potential for analysing the molecular transport in synthetic systems, with implications for designing targeted delivery platforms or biosensors. The analytical model effectively interprets the k_{leak} values obtained from the simulation, which provides a reasonable agreement between the model and the data. Fig. 5 depicts the rate constant of molecular transport dependent on pore size between GUVs with different fluorescent probes. The data points are represented by rectangle (black) for calcein, circle (red) for TRD-3k, upper triangle (green) for AF-SBTI, down-triangle (blue) for TRD-10 k, circle (cyan) for FITC-BSA, and star (orange) for TRD-40 k. The solid lines (black, red, green, blue, cyan, and orange) correspond to the fitting curve obtained by using Eq. 8 with K values of 0.0045, 0.0045, 0.0045, 0.0055, 0.0045, and 0.0055 for the respective rate constants. The curve fit closely matches the experimental data, showing how the molecular transport rate constant for each fluorescent probe varies with GUV pore size.

By validating simulation-derived k_{leak} values with experimental data, this study demonstrated the robustness of computational modelling for predicting molecular transport. The validated model provides a framework for designing nanoporous membranes tailored for applications in targeted drug

delivery, biosensing, and molecular biology. Future work could explore the effects of electric fields, varying membrane compositions, and multi-pore systems on molecular transport. Expanding to 3D simulations and incorporating dynamic environmental conditions may refine the applicability of these findings to complex biological systems, thus advancing the field of nanopore-mediated transport.

Conclusion: In this study, COMSOL simulations were used to examine molecular transport through individual nanopores in lipid membranes of GUVs. We studied the transport kinetics of molecules from inside to outside of GUVs through nanopores by varying the sizes of nanopores, fluorescent probes, and suspension areas. The transport of fluorescent probes followed a consistent single exponential growth function for all scenarios. Further, the rate constant of molecular transport decreased with larger fluorescent probe sizes, while it increased with larger suspension area, exhibited good agreement with previous experimental findings. Our simulation report provides valuable insights and a deeper understanding of the kinetics of molecular transport through nanopores in GUV membranes. This knowledge can contribute to future researches in the field of biomembranes and cellular transport phenomena. The findings elucidate the principles governing nanopore-mediated leakage and provide a predictive framework for designing membrane systems for controlled release, biosensing, and synthetic biology applications.

Statement on usage of artificial intelligence: The authors declare that they did not receive any help from Artificial Intelligence

Author's contribution: T.R., M.A., M.I.H., M.S.I, M.A.S.K. and M.K.A. designed the research. T.R. prepared the systems and performed the simulations. T.R., M.A., S.E. analyzed the data and generated figures. T.R., M.A., S.E. wrote the manuscript. M.I.H., M.S.I., M.A.S.K., M.M.B., H.T. and M.K.A. supervised the whole work. All authors contributed to writing, editing, and revision of the manuscript.

Acknowledgement: We would like to thank all the member of K. Alam Laboratory for their assistance and support.

Conflict of interest: The authors declare no competing interests.

Ethics statement: This study did not involve human participants, human data, or animal subjects, and therefore no ethics approval was required.

Funding: This research did not receive any specific grant from funding agencies in the public, commercial, or not-for-profit sectors.

REFERENCES

Ahamed, M.K., Ahmed, M. and Karal, M.A.S. 2022. Quantification of pulsed electric field for the rupture of giant vesicles with various surface charges, cholesterols and osmotic pressures. *PLoS ONE*, **17**(1): e0262555. [*https://doi.org/10.1371/journal.pone.0262555*].

Alam Shibly, S.U., Ghatak, C., Sayem Karal, M.A., Moniruzzaman, M. and Yamazaki, M. 2016. Experimental estimation of membrane tension induced by osmotic pressure. *Biophysical Journal*, **111**(10): 2190-2201.

Asaduzzaman, M., Emon, S., Ishtiaque, M.S., Hossain, M.I., Karal, M.A.S., Billah, M.M., *et al.*, 2025. Molecular transport through nano-sized multipores of lipid vesicles: a COMSOL simulation study. *European Biophysics Journal*. **54**(3–4): 159-169.

Berthier, J. and Silberzan, P. 2010. *Microfluidics for Biotechnology*. Artech House, Boston, USA.

Boukany, P.E., Morss, A., Liao, W., Henslee, B., Jung, H., Zhang, X., *et al.*, 2011. Nanochannel electroporation delivers precise amounts of biomolecules into living cells. *Nature Nanotechnology*, **6**(11): 747-754.

Casas-Rodrigo, I., Vornholt, T., Castiglione, K., Roberts, T.M, Jeschek, M., Ward, T.R. *et al.* 2025. Permeabilisation of the outer membrane of *Escherichia coli* for enhanced transport of complex molecules. *Microbial Biotechnology*, **18**(3): e70122. [*https://doi.org/10.1111/1751-7915.70122*].

Casciola, M. and Tarek, M. 2016. A molecular insight into the electro-transfer of small molecules through electropores driven by electric fields. *Biochimica et Biophysica Acta - Biomembranes*, **1858**(10): 2278-2289.

Chang, D.C. and Reese, T.S. 1990. Changes in membrane structure induced by electroporation as revealed by rapid-freezing electron microscopy. *Biophysical Journal*, **58**(1): 1-12.

Datta, A. and Rakesh, V. 2010. *An Introduction to Modelling of Transport Processes: Applications to Biomedical Systems.* Cambridge University Press, New York, USA.

Emon, S., Sakib, S., Bardhan, N., Saha, S., Asaduzzaman, M. and Alam, M.K. 2025. Molecular dynamics of electroporation and quantitative analysis of molecular transport. *Journal of Biological Physics* **51**(1): 18. [*https://doi.org/10.1007/s10867-025-09682-w*].

Gaur, A.S., Kumar, V. and Singh, D. 2014. Institutions, resources, and internationalization of emerging economy firms. *Journal of World Business*, **49**(1): 12-20.

Gómez, V., De La Pava, I. and Henao, O. 2014. Stochastic diffusion of calcium ions through a nanopore in the cell membrane created by electroporation. *Proceedings of the 2014 COMSOL Conference in Boston, USA.*

Hasan, M., Karal, M.A.S., Levadnyy, V. and Yamazaki, M. 2018. Mechanism of initial stage of pore formation induced by antimicrobial peptide magainin 2. *Langmuir*, **34**(10): 3349-3362.

Jayasooriya, V. and Nawarathna, D. 2017. Simulation of molecular transport through an electroporated cell using COMSOL Multiphysics. *13th COMSOL Conference, Boston, USA.*

Karal, M.A.S., Ahamed, M.K., Rahman, M., Ahmed, M., Shakil, M.M. and Siddique-e-Rabbani, K. 2019. Effects of electrically-induced constant tension on giant unilamellar vesicles using irreversible electroporation. *European Biophysics Journal*, **48**(8): 731-741.

Karal, M.A.S., Alam, J.M., Takahashi, T/, Levadny V and Yamazaki M. 2015. Stretch-activated pore of the antimicrobial peptide, magainin 2. *Langmuir*, **31**(11): 3391-3401.

Karal, M.A.S., Islam, M.K. and Mahbub, Z.B. 2020. Study of molecular transport through a single nanopore in the membrane of a giant unilamellar vesicle using COMSOL simulation. *European Biophysics Journal*, **49**(1): 59-69.

Karal, M.A.S., Levadnyy, V., Tsuboi, T., Belaya, M. and Yamazaki, M. 2015. Electrostatic interaction effects on tension-induced pore formation in lipid membranes. *Physical Review E*, **92**(1): 012708. [*https://doi.org/10.1103/PhysRevE.92.012708*].

Karal, M.A.S., Levadnyy, V. and Yamazaki, M. 2016. Analysis of constant tension-induced rupture of lipid membranes using activation energy. *Physical Chemistry Chemical Physics*, **18**(19): 13487-13495.

Karal, M.A.S., Rahman, M., Ahamed, M.K., Shibly, S.U.A., Ahmed, M. and Shakil, M.M. 2019. Low cost non-electromechanical technique for the purification of giant unilamellar vesicles. *European Biophysics Journal*, **48**(4): 349-359.

Karal, M.A.S. and Yamazaki, M. 2015. Communication: Activation energy of tension-induced pore formation in lipid membranes. *The Journal of Chemical Physics*, **143**(8): 081103. [*https://doi.org/10.1063/1.4930108*].

Kotnik, T., Rems, L., Tarek, M. and Miklavčič, D. 2019. Membrane electroporation and electropermeabilization: Mechanisms and Models. *Annual Review of Biophysics* **48**(1): 63-91.

Liu, F., Su, R., Jiang, X., Wang, S., Mu, W. and Chang, L. 2024. Advanced micro/nano-electroporation for gene therapy: recent advances and future outlook. *Nanoscale* **16**(22): 10500-10521.

Movahed, S. and Li, D. 2012. Electrokinetic transport through the nanopores in cell membrane during electroporation. *Journal of Colloid and Interface Science*, **369**(1): 442-452.

Nayak, S. and Herzog, R.W. 2010. Progress and prospects: Immune responses to viral vectors. *Gene Therapy*, **17**(3): 295-304.

Rahman, F., Halder, S., Rahman, S. and Hossen, M.L. 2025. Investigating the therapeutic ability of novel antimicrobial peptide dendropsophin 1 and its analogues through membrane disruption and monomeric pore formation. *The Journal of Physical Chemistry B*, **129**(12): 3171-3182.

Rawicz, W., Olbrich, K.C., McIntosh, T., Needham, D. and Evans, E. 2000. Effect of chain length and unsaturation on elasticity of lipid bilayers. *Biophysical Journal*, **79**(1): 328-339.

Roiter, Y., Ornatska, M., Rammohan, A.R., Balakrishnan, J., Heine, D.R. and Minko, S. 2008. Interaction of nanoparticles with lipid membrane. *Nano Letters*, **8**(3): 941-944.

Roy, S.K., Karalm M.A.S., Kadir, M.A. and Rabbani, K.S. 2019. A new six-electrode electrical impedance technique for probing deep organs in the human body. *European Biophysics Journal*, **48**(8): 711-719.

Saitoh, A., Takiguchi, K., Tanaka, Y. and Hotani, H. 1998. Opening-up of liposomal membranes by talin. *Proceedings of the National Academy of Sciences*, **95**(3): 1026-1031.

Sengel, J.T. and Wallace, M.I. 2016. Imaging the dynamics of individual electropores. *Proceedings of the National Academy of Sciences*, **113**(19): 5281-5286.

Sharmin, S., Islam, M.Z., Karal, M.A.S., Alam Shibly, S.U., Dohra, H. and Yamazaki, M. 2016. Effects of lipid composition on the entry of cell-penetrating peptide oligoarginine into single vesicles. *Biochemistry*, **55**(30): 4154-4165.

Sikorska, E., Iłowska, E., Wyrzykowski, D. and Kwiatkowska, A. 2012. Membrane structure and interactions of peptide hormones with model lipid bilayers. *Biochimica et Biophysica Acta (BBA) - Biomembranes*, **1818**(12): 2982-2993.

Sözer, E.B., Haldar, S., Blank, P.S., Castellani, F., Vernier, P.T. and Zimmerberg, J. 2020. Dye transport through bilayers agrees with lipid electropore molecular dynamics. *Biophysical Journal*, **119**(9): 1724-1734.

Spugnini, E.P., Arancia, G., Porrello, A., Colone, M., Formisano, G., Stringaro, A., *et al.*, 2007. Ultrastructural modifications of cell membranes induced by "electroporation" on melanoma xenografts. *Microscopy Research and Technique*, **70**(12): 1041-1050.

Stewart, M.P., Sharei, A., Ding, X., Sahay, G., Langer, R. and Jensen, K.F. 2016. *In vitro* and *ex vivo* strategies for intracellular delivery. *Nature*, **538**(7624): 183-192.

Tamba, Y., Ariyama, H., Levadny, V. and Yamazaki, M. 2010. Kinetic pathway of antimicrobial peptide magainin 2-induced pore formation in lipid membranes. *The Journal of Physical Chemistry B*, **114**(37): 12018-12026.

Tamba, Y. and Yamazaki, M. 2005. Single giant unilamellar vesicle method reveals effect of antimicrobial peptide magainin 2 on membrane permeability. *Biochemistry*, **44**(48): 15823–15833.

Tamba, Y. and Yamazaki, M. 2009. Magainin 2-induced pore formation in the lipid membranes depends on its concentration in the membrane interface. *The Journal of Physical Chemistry B*, **113**(14): 4846-4852.

Tanaka, T., Tamba, Y., Masum, S.M., Yamashita, Y. and Yamazaki, M. 2002. La3+ and Gd3+ induce shape change of giant unilamellar vesicles of phosphatidylcholine. *Biochimica et Biophysica Acta (BBA) - Biomembranes*, **1564**(1): 173-182.

Teissie, J. 2017. Membrane permeabilization lifetime in experiments. pp. 61–75. **In:** *Handbook of Electroporation*. Miklavčič D(Ed). Cham: Springer International Publishing, Chams, Switzerland.

Vargason, A.M., Anselmo, A.C. and Mitragotri, S. 2021. The evolution of commercial drug delivery technologies. *Nature Biomedical Engineering*, **5**(9): 951-967.

Yamashita, Y., Masum, S. Md., Tanaka, T. and Yamazaki, M. 2002. Shape changes of giant unilamellar vesicles of phosphatidylcholine induced by a de novo designed peptide interacting with their membrane interface. *Langmuir*, **18**(25): 9638-9641.

Zasloff, M. 2002. Antimicrobial peptides of multicellular organisms. *Nature*, **415**(6870): 389-395.